Biochemistry and Biophysics Reports 42 (2025) 101995

Contents lists available at ScienceDirect

Biochemistry and Biophysics Reports

journal homepage: www.elsevier.com/locate/bbrep

Molecular modeling approach in design of new scaffold of α-glucosidase inhibitor as antidiabetic drug

Fatemeh Amini, Khansa Ismaeal Abbas, Jahan B. Ghasemi *

School of Chemistry, University College of Science, University of Tehran, P.O. Box 14155-6455, Tehran, Iran

ARTICLE INFO

Keywords:
α-Glucosidase inhibitors
Structure-based drug design
3D-QSAR
Pharmacophore modeling
Molecular dynamics simulation

ABSTRACT

Targeting α-glucosidase is essential for diabetes treatment, as it inhibits carbohydrate breakdown in the small intestine, helping to control blood glucose levels. This study aimed to design and computationally analyze sugar-based compounds as potent α-glucosidase inhibitors. We screened the BindingDB database with pharmacophore modeling in Pharmit, achieving an enrichment factor of 50.6, and evaluated ligand binding through molecular docking simulations, identifying key functional groups for optimal interactions. The compound 1b demonstrated strong inhibitory potential, binding to residues similar to those targeted by acarbose, with a GoldScore fitness of 60.57 compared to acarbose's 50.56 (IC_{50} = 0.750 nM). A subset of compounds underwent 3D-QSAR modeling, revealing functional groups that enhance inhibitory activity, supported by high statistical quality (q^2 of 0.571, r^2 of 0.926, and F-values of 62.569 for CoMFA and 51.478 for CoMFA-RF). Based on these findings, we designed a novel scaffold through scaffold hopping, incorporating a glycosyl group to target the enzyme's active site, an amine group to improve binding affinity, and two phenyl groups that enhance inhibitory activity. Molecular docking and dynamics simulations further validated the stability and efficacy of this scaffold, showing superior interaction with α-glucosidase compared to acarbose. ADME property predictions suggested favorable pharmacokinetic properties, supporting this scaffold's potential for development as a diabetes treatment.

1. Introduction

Diabetes is a metabolic disorder characterized by high blood glucose level, which can precipitate other serious diseases such as cancer and cardiovascular diseases [1]. The prevalence of diabetes has been escalated due to lifestyle changes, unhealthy dietary habits, and obesity [2]. Diabetes has two main types, including type 1 and type 2 diabetes. The body does not produce enough insulin in Type 1, and in Type 2 it cannot use insulin properly [3]. The main therapeutic strategy for managing diabetes entails maintaining optimal blood glucose levels, which helps mitigate the associated complications [4]. One effective treatment approach for type 2 diabetes involves inhibiting carbohydrate degradation through the suppression of carbohydrate-hydrolyzing enzymes, such as pancreatic α-amylase and intestinal α-glucosidase [5].

α-Glucosidase (EC 3.2.1.20) is an enzyme found on the intestinal brush border membrane that breaks down complex sugars to absorbable monosaccharides like D-glucose [6]. α-Glucosidase inhibitors (AGIs) such as acarbose, miglitol, and voglibose (Scheme I) are frontline drugs for managing type 2 diabetes [7]. Acarbose, the first approved drug in the AGI category, operates by retarding the release of glucose from polysaccharides through binding to the active α-glucosidase site. Nevertheless, the existence of certain side effects associated with commonly-used drugs, coupled with the imperative of establishing personalized drug databases for the future, has engendered ongoing endeavors in the pursuit of novel AGIs.

Given the growing prevalence of diabetes and the limitations of current therapies, this study aimed to design novel sugar-based α-glucosidase inhibitors using advanced computational methodologies. Specifically, we sought to employ a combination of pharmacophore modeling, 3D-QSAR, molecular docking, and scaffold hopping to design potent inhibitors with favorable pharmacokinetic properties. The primary objective of this work is to identify a novel scaffold with improved α-glucosidase inhibitory potential while reducing adverse effects compared to existing AGIs, thereby providing a promising therapeutic candidate for type 2 diabetes management.

Computer-aided drug design (CADD) has become a pivotal tool in rational drug discovery, offering a cost-effective approach to accelerating the identification of promising drug candidates [8]. This

* Corresponding author.
E-mail address: jahan.ghasemi@ut.ac.ir (J.B. Ghasemi).

https://doi.org/10.1016/j.bbrep.2025.101995
Received 1 January 2025; Received in revised form 24 March 2025; Accepted 27 March 2025

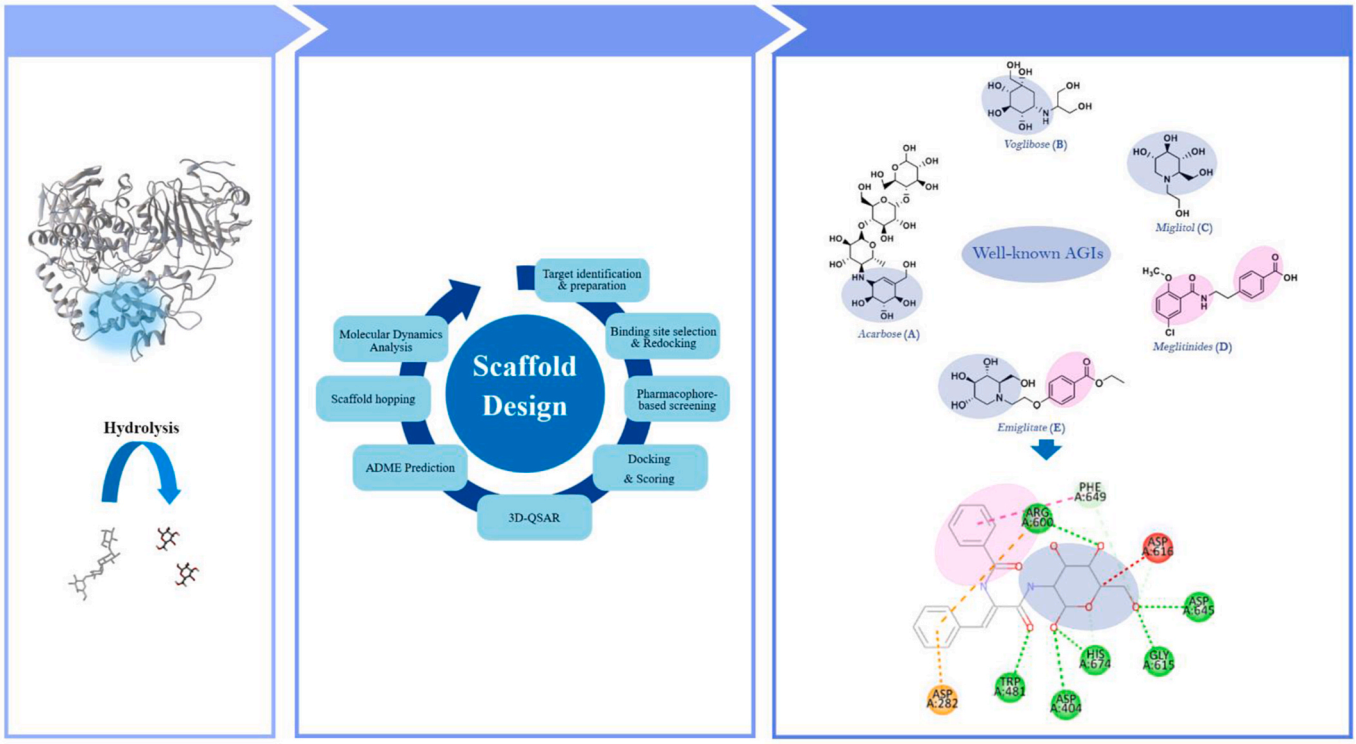

Scheme 1. In Silico Scaffold Design of α-Glucosidase Inhibitors Using a Comprehensive Computational Approach.

computational strategy leverages chemical, molecular, and quantum principles to design molecules with high therapeutic potential. CADD methodologies are broadly classified into structure-based and ligand-based approaches. Structure-based drug design (SBDD), for instance, utilizes the structural data of target macromolecules to guide the design of ligands with optimized binding affinities [9].

Pharmacophore modeling identifies essential spatial features that facilitate drug-target interactions, laying the groundwork for novel drug discovery. Meanwhile, quantitative structure-activity relationship (QSAR) analysis examines the impact of molecular substituents within a fixed framework, correlating structural variations with biological activity. Together, pharmacophore modeling and QSAR can effectively guide the design of compounds with enhanced biological potency. Molecular docking, when paired with molecular dynamics simulations (MD), further refines this process by predicting binding affinities, analyzing conformational stability, and detailing protein-ligand interactions. This combination aids in the efficient selection of lead compounds by simulating the dynamic behavior of protein-ligand complexes, revolutionizing drug design [10]. Scaffold hopping, a key technique for designing novel agents, involves analyzing and comparing core structures to generate derivatives with improved efficacy. After selecting promising scaffolds, their potential as viable drugs can be assessed by evaluating physicochemical, ADME (absorption, distribution, metabolism, excretion), and drug-likeness properties.

Despite numerous advancements, gaps remain in understanding the specific structural features that govern the inhibitory efficacy of α-glucosidase inhibitors. Recent studies have explored synthetic and natural compounds with α-glucosidase inhibitory potential, such as pyranoquinolinyl derivatives, flavonoids, and triazole compounds [11–14]. However, these studies often lack detailed computational validations or focus narrowly on specific chemical classes. Our research aims to address these gaps by leveraging a comprehensive computational approach that integrates advanced modeling techniques to identify and optimize novel scaffolds.

2. Materials and methods

2.1. Software

Molecular docking calculations were conducted using the GOLD (Genetic Optimization for Ligand Docking, version 5.3.0) program. The receptor-ligand pharmacophore generation module in Discovery Studio 4.1 (DS) was used to identify critical features α-glucosidase binding with acarbose. Pharmacophore-based screening was conducted using the Pharmit web server on the initial dataset for extract compounds contained a sugar-based substructure based on a user-defined pharmacophore hypothesis. The 3D-QSAR modeling was performed on refined dataset using SYBYL 7.3.

2.2. Data preparation

The crystal structure of the α-glucosidase and α-amylase enzymes (PDB_ID: 5NN8, 3BAJ) were obtained from the Protein Data Bank. Automated preparation tools in DS were used to assign missing atoms, optimize hydrogen-bonding networks, and remove water molecules to prevent non-specific interactions. The CHARMm force field was applied to ensure accurate minimization of target. Parameters such as energy cut-off (0.9) and pH (7.4) were chosen to replicate physiological conditions and ensure biologically relevant interactions. 493 Ligands with IC_{50} values against α-glucosidase were collected from BindingDB (https://www.bindingdb.org) as initial dataset and similarly optimized by energy minimizing and assigning hydrogens.

2.3. Molecular docking

GOLD employs the Lamarckian genetic algorithm to dock flexible ligands into receptor binding sites, allowing exploration of ligand conformational flexibility with partial receptor flexibility to ensuring accurate docking results [15]. The GoldScore fitness function was utilized to assess ligand-protein binding affinities [16]. To validate the

docking performance and accuracy, the native co-crystallized ligand and acarbose from the crystal structures of the α-glucosidase binding site were subjected to flexible docking. Docking parameters for α-glucosidase were validated by re-docking acarbose in the binding site of the crystalline protein. A maximum of 10 docking GA runs per molecule was employed, yielding 1.5 Å RMS deviations. The validated docking parameters were then saved with default structural parameters for subsequent steps of the docking study. The active site consisted of Asp616, Phe649, Trp613, Met519, Arg520, Arg600, Asp404, His674, Asp324, His594, and Asp518. The 3D structures of the compounds were downloaded and imported into DS. Partial charges were calculated using the Momany-Rone option, followed by the Smart Minimizer algorithm with 2000 steps of steepest descent and an RMS gradient tolerance of 0.01, succeeded by Conjugate Gradient minimization. Subsequently, all compounds were docked into the active site using GOLD, with GoldScore serving as the scoring function. The molecular docking study compared new AGIs and identified the most promising inhibitors.

2.4. Pharmacophore development

The pharmacophore modeling and pharmacophore-based screening utilized with the DS receptor-ligand pharmacophore generation and Pharmit search engine, respectively. The receptor-ligand pharmacophore generation protocol in DS employed the catalyst/HipHop algorithm to generate common features among a set of active ligands. Additionally, inactive compounds were used to add excluded volumes to the pharmacophore model. The pharmacophore model aims to provide steric and electrostatic features essential for optimal interaction with a specific biological target [17]. Next, the 3D structure of acarbose (reference ligand) in complex with α-glucosidase was extracted to generate a pharmacophore model with 10 maximum and 4 minimum features, a lowest inter-feature distance of 2.0 Å, maximum omitted features of 1, and a rigid fitting method. The Pharmit module selected for its efficiency in rapid screening large compound libraries using a user-defined pharmacophore hypothesis, enabling the identification of candidate compounds with optimal spatial and chemical properties. To generate decoys, five of the most active compounds were selected from initial dataset and used DUDE (http://dude.docking.org/generate). The Pharmit algorithm assessed different combinations of features, using the enrichment factor as an objective function to identify the best combination of features. We incorporate six pharmacophore features include hydrogen bond acceptor (HBA), hydrogen bond donor (HBD), aromatic ring, hydrophobic group, positive ionizable, and negative ionizable groups to screen initial dataset [18].

2.5. 3D-QSAR

Quantitative structure-activity relationship techniques are widely used in various fields, including drug design, toxicity prediction, and molecular system property screening. Recently, 4D, 5D, and 6D formalisms have introduced new dimensions to QSAR analysis [19]. In this study, predictive 3D-QSAR CoMFA and CoMFA-RF (Region Focusing) models were applied to the entire dataset using the SYBYL 7.3 molecular modeling software program from Tripos, Inc (St. Louis, MO). CoMFA analysis establishes correlations between the dataset's biological activities and their 3D structures. The dataset comprised 97 compounds with a sugar-based substructure, their IC_{50} values were converted to pIC_{50}, and 37 compounds were selected with a minimum numerical difference of 0.1 unit of pIC_{50} for further analysis in SYBYL. Energy minimization was conducted using the Tripos force field and a Powell conjugate gradient algorithm with specific convergence criteria. Partial atomic charges were calculated using the Gasteiger–Huckel method. All molecules shared a common sugar-based substructure, with compound 1b serving as the main scaffold for alignment purposes. Efficient and robust alignment of the compounds is crucial for the model's accuracy [20]. A field-fit method was utilized for alignment based on minimizing RMSD due to the six rigid body degrees of freedom and/or any user-specified torsion angles [21]. In the CoMFA method, the aligned molecules were placed at the center of a 3D-grid box with dimensions of 2.0 Å using a sp^3 hybridized carbon atom as a probe with a +1.0 charge to calculate steric and electrostatic interaction fields. The Coulomb and Lennard–Jones potential functions estimated steric and electrostatic interactions, respectively. Column filtering was set to 2 kcal/mol to reduce noise and improve the signal-to-noise ratio, and the intended cut-off for computing steric and electrostatic fields was 30 kcal/mol. To optimize the field sampling, an all-orientation search (AOS) and all position search (APS) were implemented in SYBYL programming language (SPL). This systematic rotation of the molecular aggregate selected the best orientation and position of aligned molecules in the grid box space to achieve the highest q^2 value [20]. Additionally, the CoMFA region

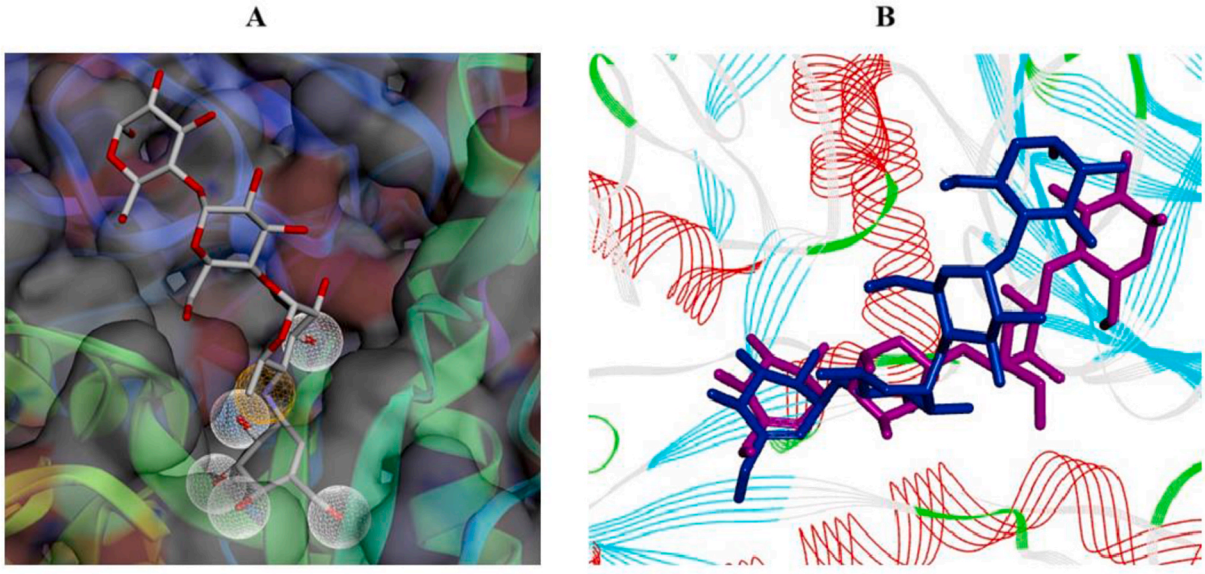

Fig. 1. A) Representation of six pharmacophore features derived from the acarbose complex with α-glucosidase enzyme crystal structure. White present HBD features, and orange present HBA features. B) Overlap of redocked (blue) and crystallographic (purple) acarbose inside the cavity of α-glucosidase for validation of docking simulation.(For interpretation of the references to colour in this figure legend, the reader is referred to the web version of this article.)

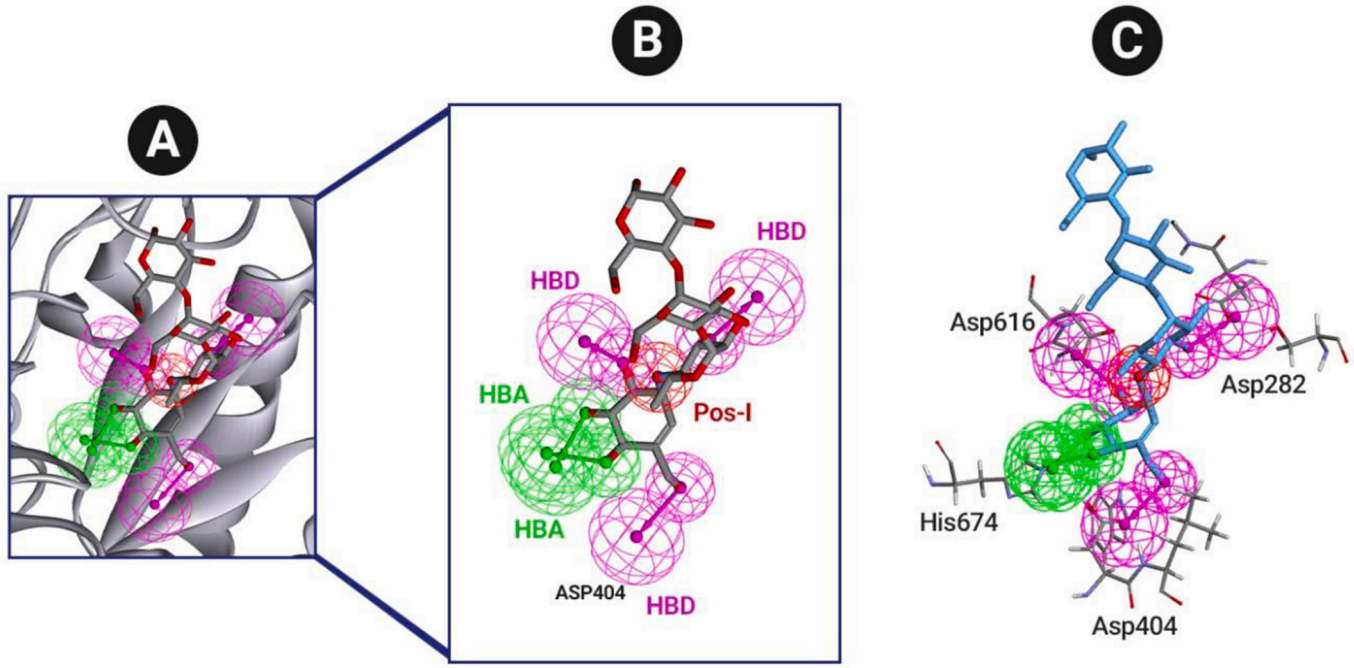

Fig. 2. Representation of pharmacophore features, A) based on the acarbose interactions inside the α-glucosidase cavity. B) important features showed HBA and HBD, and positive ion (Pos-I). C) important residues of cavity.

focusing (CoMFA-RF) method was employed to refine the model and enhance the contribution of lattice points most relevant to the model. The developed models successfully correlated structural features with biological activity, revealing essential parameters required for activity prediction.

2.6. Molecular dynamics simulation

Molecular dynamics (MD) simulation is a robust computational technique for assessing macromolecular flexibility and analyzing biological functions through internal motions [22]. In this study, the best pose from docking and the newly designed scaffold against α-glucosidase and α-amylase; underwent 100 ns MD simulations using the GROMACS 2024.4 with the 54a7 GROMOS force field and the SPC explicit solvation model. Comparative MD simulations were also performed for acarbose and the apo form (protein in water). Input files for MD were generated with separate coordinate and topology files for each ligand and protein. The ligands were optimized using the Automated Topology Builder (ATB) [23], while α-glucosidase was prepared using MOE to add missing residues and verify protonation states [24]. The complexes were placed in a 1 Å octahedral box, solvated, and neutralized with NaCl at 300 K and 1 atm. System energy minimization was performed using the steepest descent algorithm, followed by 1 ns of NVT and NPT equilibration. The cut-off method and Particle-Mesh Ewald (PME) were applied for van der Waals and long-range electrostatic interactions. MD simulations evaluated the stability of protein-ligand interactions and validated docking results by analyzing RMSD, RMSF, radius of gyration (R_g), hydrogen bond dynamics, and solvent-accessible surface area (SASA). Visualization and data analysis were performed using Visual Molecular Dynamics (VMD) and Xmgrace, enabling a comprehensive comparison across simulations. Additionally, binding free energy calculations were conducted using the molecular mechanics Poisson–Boltzmann surface area (MM-PBSA) method. The binding free energy was determined as the difference between the complex and the sum of the isolated protein and ligand energies, incorporating potential energy (electrostatic and van der Waals contributions) and solvation free energy (polar and nonpolar components). The g_mmpbsa tool was used to compute average binding free energy values.

3. Results and discussion

3.1. Pharmacophore analysis

An α-glucosidase enzyme-acarbose (as a drug reference) complex with ligand was used to make a receptor-ligand pharmacophore model. It was then docked into the cavity and loaded in Pharmit. A library including 5 of the most active compounds and decoys was built, and different combinations of features were tested. The pharmacophore model enrichment factor was 50.6 with 5 HBDs from OH and a HBA from NH group (Fig. 1A).

The receptor-ligand pharmacophore modeling method in DS was used to generate 10 hypotheses, then compared with a Pharmit pharmacophore model, and the best results were reported (Fig. 2). The results demonstrate that the selected features align with the Pharmit pharmacophore model, highlighting the importance of sugar-based structures within the enzyme cavity for biological activity. The model identifies HBD and HBA as key contributors, consistent with α-glucosidase's role in oligosaccharide hydrolysis. For model construction, 97 compounds from the Binding Database, including the most active compound (IC_{50} = 6 nM), were utilized, each sharing a common substructure.

After examining all the hypotheses of the pharmacophore model in DS and the Pharmit, it can be concluded that there is not much difference between the hydrogen bond interactions of the donor or acceptor in the glucose-base substitution placed inside the cavity. This means the important features with the mentioned angles and distance are necessary to allow hydrogen interactions, and their type is not very important.

3.2. Molecular docking analysis

Molecular docking constitutes a vital approach in SBDD, facilitating the prediction of a ligand's principal binding mode(s) with a protein of established 3D structure [16]. α-glucosidase was prepared and acarbose was docked into its cavity to validate docking parameters and used for

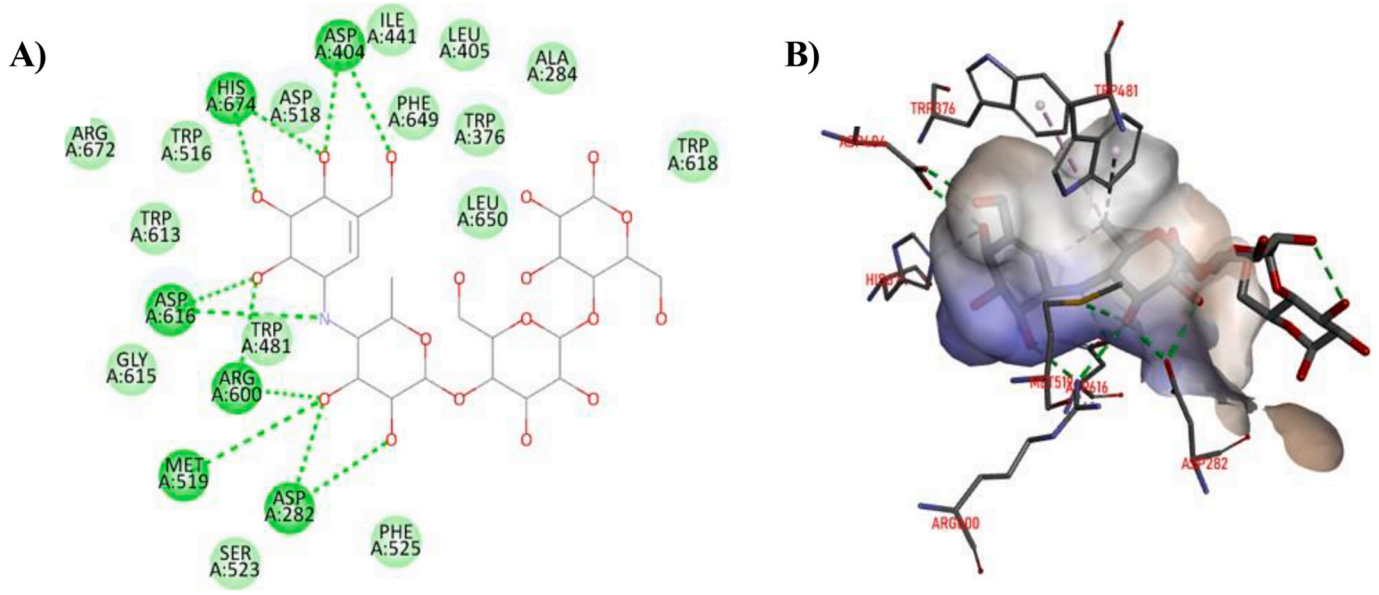

Fig. 3. A) 2D-diagram of acarbose and B) 3D-diagram interactions of acarbose bind in active site of α-glucosidase. Green dash-lines indicate hydrogen bonds interactions.(For interpretation of the references to colour in this figure legend, the reader is referred to the web version of this article.)

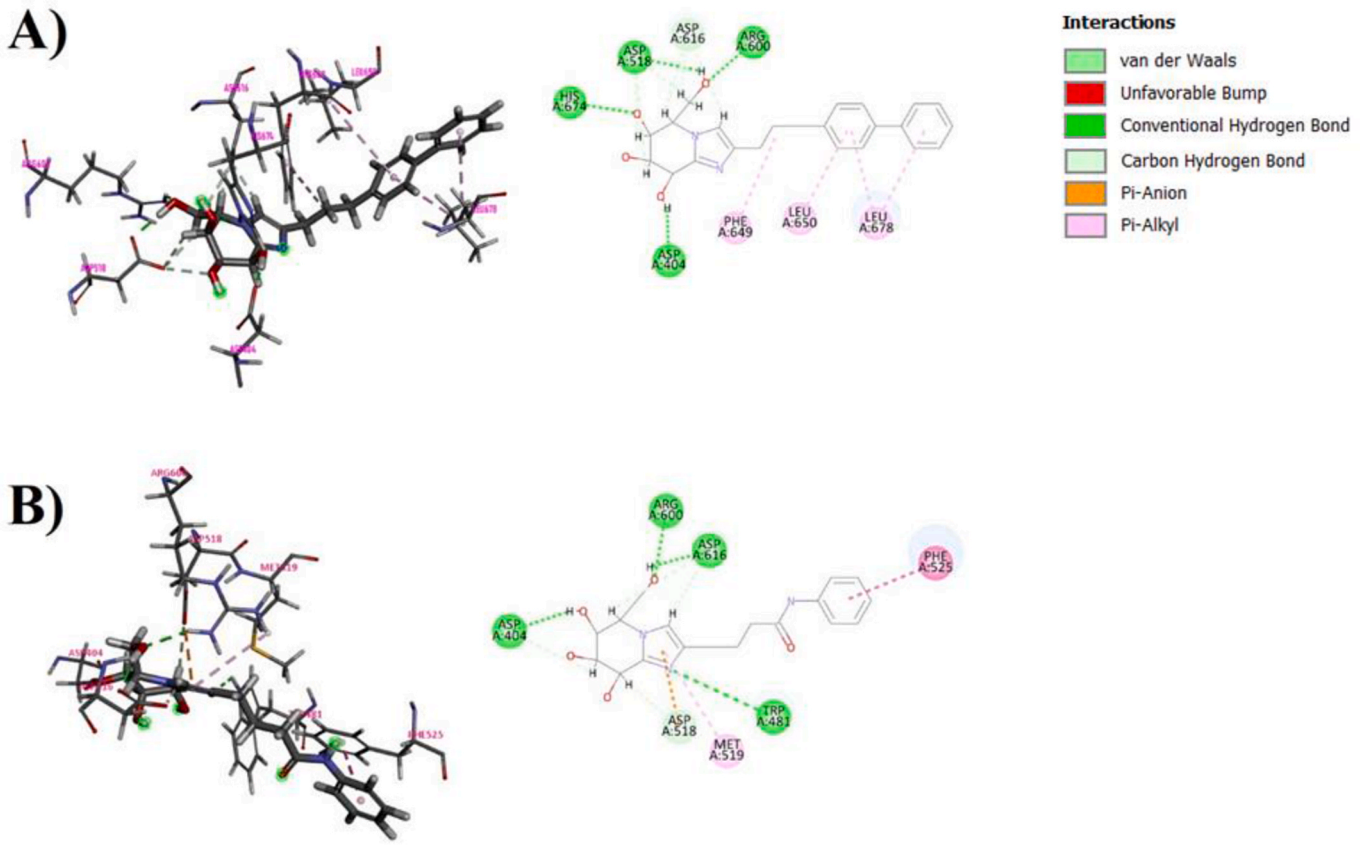

Fig. 4. 2D and 3D interactions of potent ligands with the highest GoldScore fitness. A) compound 1b and B) compound 7b showed similar interactions and high GoldScore.

next steps. Re-docking of acarbose showed an almost similar interaction to its matching crystallographic conformation (RMSD = 2.87) and a GoldScore fitness of 50.56, declaring the selected parameters acceptable (Fig. 1B).

The rational design of inhibitors for this protein hinges on the sugar structure, wherein acarbose's internal connection within the active site sets it apart from the external components. In light of this, we proposed a novel structure with enhanced activity and reduced complications.

Initially, we precisely characterized the binding elements of acarbose within the active site of α-glucosidase (Fig. 3). Notably, hydrogen bonds were identified between the oxygen of the hydroxyl group and the nitrogen of the amine group with Asp404, His674, Asp616, Arg600,

Table 1
Summary of the results of PLS analysis of QSAR model.

Component	CoMFA	CoMFA-RF
q^2	0.571	0.561
R^2	0.926	0.911
F value	62.569	51.478
RMSEC	0.427	0.467
n	1	1
RMSEP	0.951	0.965
Fraction		
Steric	0.5	
Electrostatic	0.5	

q^2: cross validated correlation coefficient after the leave-one-out procedure; R^2: non cross validated correlation coefficient; F value: degree of statistical confidence; RMSEC: root-mean-square-error of calibration; n: optimum number of components; RMSEP: root-mean-square-error of prediction.

Met519, and Asp282. Additionally, well-established hydrophobic interactions were observed with Trp481, Trp376, Asp404, His674, Met519, and Asp616.

Among the tested compounds, the most active one, compound 1b, exhibited the best GoldScore fitness (60.6), correctly predicting its potency against α-glucosidase. Fig. 4A highlights the formation of hydrogen bonds between three OH groups and Arg600, Asp518, His674, and Asp404 in the active site, mirroring those present in acarbose's sugar structure within the cavity. Similarly, Fig. 4B depicts hydrogen bond interactions between OH groups and Arg600, Asp616, Asp404, and Trp481 for compound 7b in the active site, resembling acarbose's glycosyl fragment interactions. compound 7b demonstrated hydrogen bond interactions with Asp616, Arg600, Asp518, and Asp404 in the sugar-based structure, but fewer interactions within the cavity, leading to lower GoldScore fitness and activity compared to other compounds. Similarly, Molecular docking of compound 5e confirmed desired interactions with certain residues, but an unfavorable OH interaction with Asp404 resulted in a lower GoldScore fitness compared to 1b. The GoldScore fitness values for the docked compounds are provided in Table S5, revealing an overall trend that aligns the scores and activities with the correct prediction of Docking Gold. This establishes a significant correlation between the compound's structure, protein interactions, and GoldScore fitness values. However, it is essential to consider an error range of approximately 0.5–1.

3.3. 3D-QSAR

3.3.1. PLS analysis

In this study, we constructed CoMFA (Comparative Molecular Field Analysis) and CoMFA- RF (Region Focus) models to assess the reliability of the 3D-QSAR model. PLS (Partial Least Squares) analysis of CoMFA and CoMFA-RF datasets yielded q^2 values of 0.571 and 0.561, respectively, indicating the robustness of these models (see Table 1). The standard error of estimate (SEE) for CoMFA and CoMFA-RF was found to be 0.427 and 0.467, while the r^2 values were 0.926 and 0.911, respectively. The Fischer ratio (F-values) for CoMFA and CoMFA-RF were 62.569 and 51.478, respectively, with a column filtering of 2 kcal/mol for both models. Based on the comparison of PLS results, the CoMFA model outperforms CoMFA-RF due to its larger number of compounds and continuous data range with closely clustered IC_{50} values. The CoMFA model underwent an initial analysis without any processing and was further optimized using the rotation program (AOS) to achieve the highest q^2 value. Ultimately, the dataset position and rotation yielding an initial q^2 value of 0.571 were determined to be the most favorable.

3.3.2. Contour map analysis

Contour map analysis was employed to visualize the interaction between inhibitors and target proteins using the 3D-QSAR models. CoMFA contour maps provided insights into the steric and electrostatic fields. Green and blue contours represent favorable regions in terms of steric and electrostatic features, respectively, while yellow and red contours indicate unfavorable regions. The contribution of these contours is 80 % for steric and 20 % for electrostatic features. All contour models and their interpretations are discussed in subsequent sections. Notably, the 3D-contours of steric and electrostatic fields for the CoMFA model on the most active compound (1b) were analyzed. Acarbose contour maps served as a reference for comparing other compound contours. It is observed that there are no contours around the glycosyl group (used for alignment), confirming the accuracy of the model. The absence of contours on the continuation glucose implies that only the glycosyl group is bonded to the active site, while the continuation groups are situated outside (Fig. 5).

By analyzing the contour maps of the most active compound (1b) in Fig. 6A, green contours suggest that bulky groups in the phenyl substituent region, extending to the second ring and amine from the imidazole group, can enhance the compound's biological activity. There are

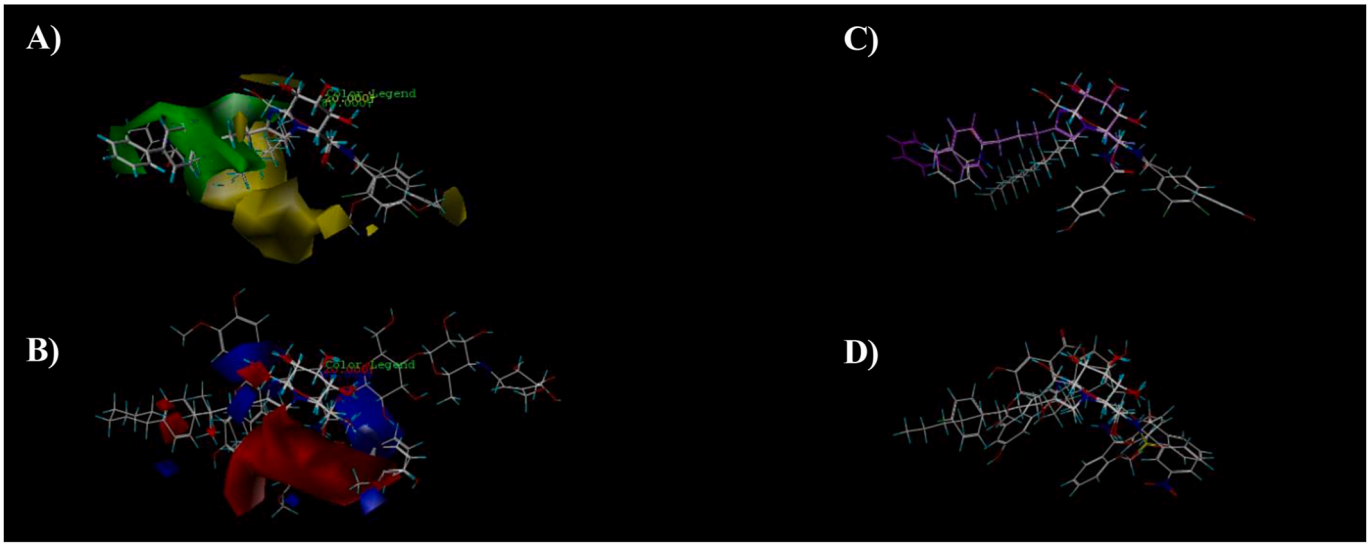

Fig. 5. A) Steric map of CoMFA and B) Electrostatic map of CoMFA on all compounds with favorable green and blue contours, respectively. C) All compound aligned on the 1b compound which is marked in purple color in the map. D) All compound contour maps.(For interpretation of the references to colour in this figure legend, the reader is referred to the web version of this article.)

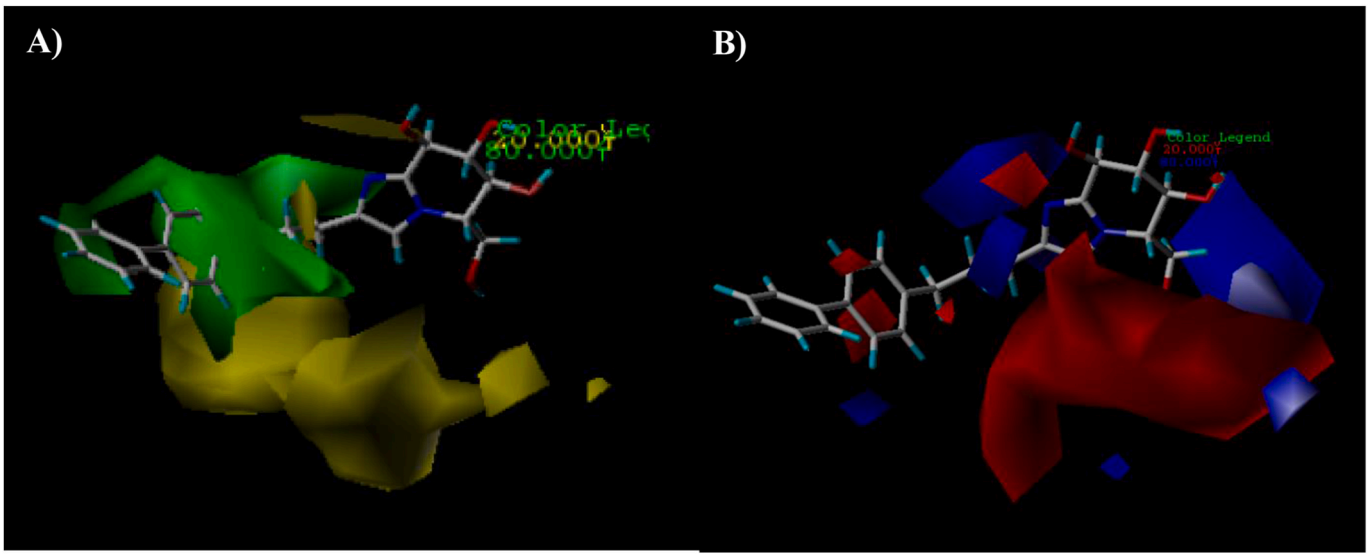

Fig. 6. CoMFA contour maps based on compound 1b. A) Steric (with favorable contour on phenyl group and without unfavorable contours) and B) Electrostatic (without any favored and unfavored contours).

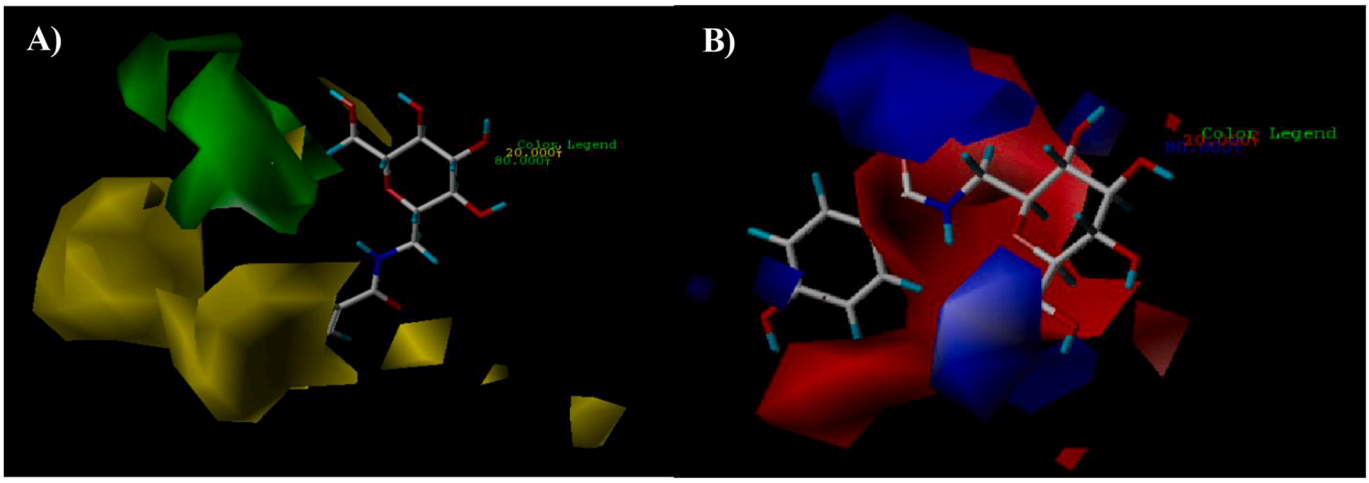

Fig. 7. CoMFA contour maps based on compound 50438511 (Binding database ID) with lowest pIC_{50}. A) Steric (with unfavored contours around phenolic cycle and without favored contours) and B) Electrostatic (with unfavored contours on amide group to phenolic cycle and without favored contours).

no terms with yellow contours to place small groups in these areas. A comparison between compound 1b and acarbose shows that 1b is more active, indicating the existence of bulky groups in the active site and forming favorable interactions with residues. Fig. 6B shows no unfavorable groups (red contours) on this compound. Therefore, the biological activity of compound 1b is higher than that of acarbose. All other compounds reported by Li Z. et al. (2013) showed very high inhibition activity with the same bulky constituents in the same part of the molecular structures.

Compound 50438511 has minor inhibition activity due to the small size of the molecule and unfavored contours on phenolic cycle and without any favored contours of steric and electrostatic (Fig. 7). Moreover, the same factor is confirmed by interpreting other compounds with the lowest IC_{50} values. The final interpretation results of the contour maps are shown in Fig. 8, which show the presence of electron-donating groups such as phenyl after the glucose scaffold increases the biological activity.

3.4. *In silico ADME and drug-likeness evaluation*

Many drug design compounds fail during clinical trials due to poor pharmacokinetic parameters [18]. To assess the potential of the top-scored compounds (GoldScore fitness >50), we evaluated their pharmacokinetic properties, including drug-likeness and ADME (Absorption, Distribution, Metabolism, and Excretion), using SwissADME online tools (http://www.swissadme.ch/index.php). ADME properties encompass the ideal characteristics required for an oral drug, ensuring rapid and complete absorption from the gastrointestinal (GI) tract, specific distribution to its target, metabolism that does not rapidly eliminate its activity, and appropriate removal without causing harm [17]. Absorption predictions were based on water solubility, lipophilicity, human intestinal absorption percentage, and permeability properties. The selected compounds exhibited water solubility (ESOL log S) within the range of −0.87 to −3.92, indicating moderate to good water solubility due to the presence of hydrophilic groups. Lipophilicity, measured as the logarithm of the n-octanol/water partition coefficient (log Po/w), ranged from −1.32 to 3.00, indicating lower to moderate lipophilicity (recommended range: $-0.7 < \text{XLOGP3} < +5.0$). While

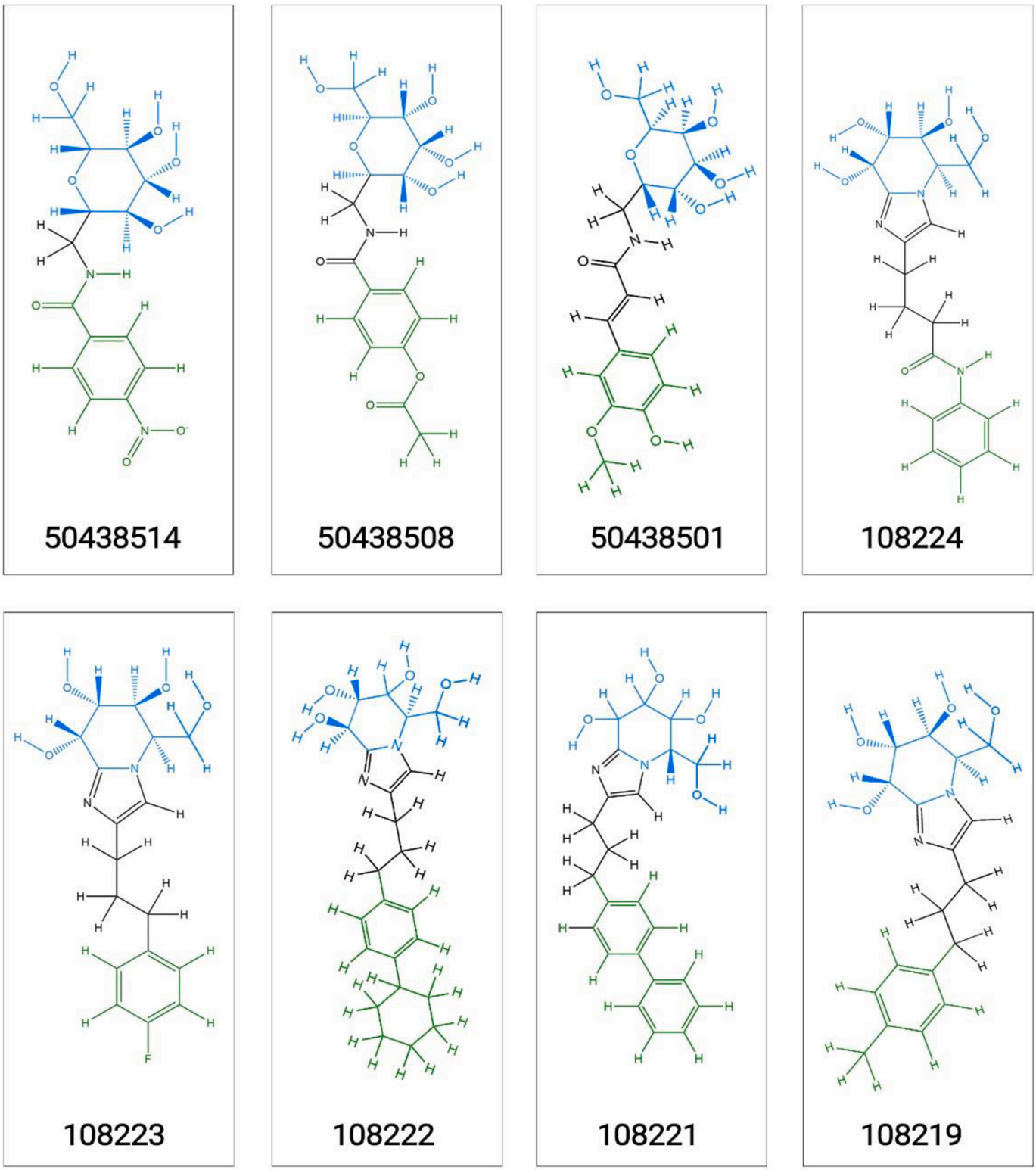

Fig. 8. The 2-dimensional structures of the most active compounds witch the common structure is marked with blue color and the favorable substitutions are marked with green color.(For interpretation of the references to colour in this figure legend, the reader is referred to the web version of this article.)

compounds 7b, 3e, and 1e fell outside this range, it is important to note that the small intestine, with a larger surface area and more permeable membranes, plays a crucial role in the absorption of orally-administered drugs [16]. Considering that α-glucosidase is an intestinal enzyme and acarbose has low intestinal absorption, the selected compounds (1b, 2b, 3b, 4b, 5b, 6b, 7b, 1d, 1c, and 2c) demonstrated high gastrointestinal absorption, indicating potential for improved inhibitory activity. Flexibility, represented by the number of rotatable bonds, should ideally be between 0 and 9. Among the compounds, 1c, 2c, 1e, 2e, 5e, and 1f had more than 9 rotatable bonds. The Csp^3 fraction, indicating the number of sp^3 carbon atoms and estimating reactivity (more saturation implies less reactivity), was found to be within the recommended range of 0.25–1 for

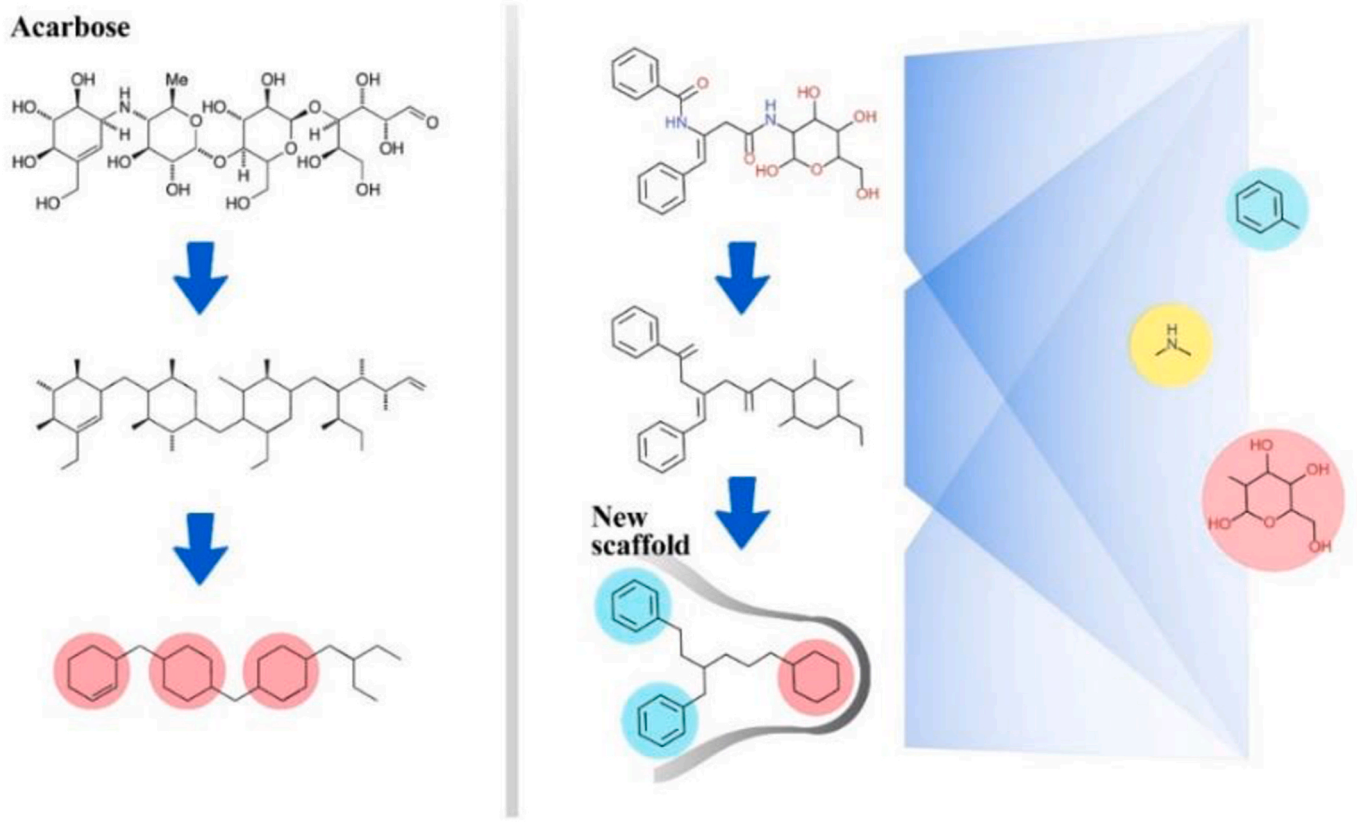

Fig. 9. Illustrates the scaffold hopping of the newly designed compound based on the fragment replacement approach.

all compounds, indicating suitable oral bioavailability. The polarity index, based on topological polar surface area (TPSA), was calculated, and compounds 1b, 2b, 3b, 4b, 5b, 6b, 7b, 1c, 2c, and 4d fell within the normal range of 20 $Å^2$ < TPSA <130 $Å^2$. The distribution of selected compounds was evaluated based on glycoprotein P (P-gp) substrate and blood-brain barrier (BBB) factors, which are determined by permeability, plasma, and brain tissue binding, influencing compound distribution in the body. None of the compounds demonstrated BBB permeation. P-gp is a crucial cell membrane protein responsible for pumping various foreign substances out of cells, distributed in the intestinal epithelium, liver cells, proximal tubule of the kidney, and capillary endothelial cells of the blood-brain barrier and blood-testis barrier. Regarding metabolism, the main cytochromes (CYP) of the P450 family were considered, with therapeutic compounds being substrates for five major isoforms: CYP1A2, CYP2C19, CYP2C9, CYP2D6, and CYP3A4. All selected compounds showed no inhibition of CYP2C9 and CYP2C19. However, compounds 3b, 4b, and 5b were found to metabolize CYP1A2, which plays a significant role in drug metabolism, cholesterol synthesis, and lipid synthesis. Compounds 1b and 2b inhibited CYP2D6, responsible for metabolizing approximately 25 % of

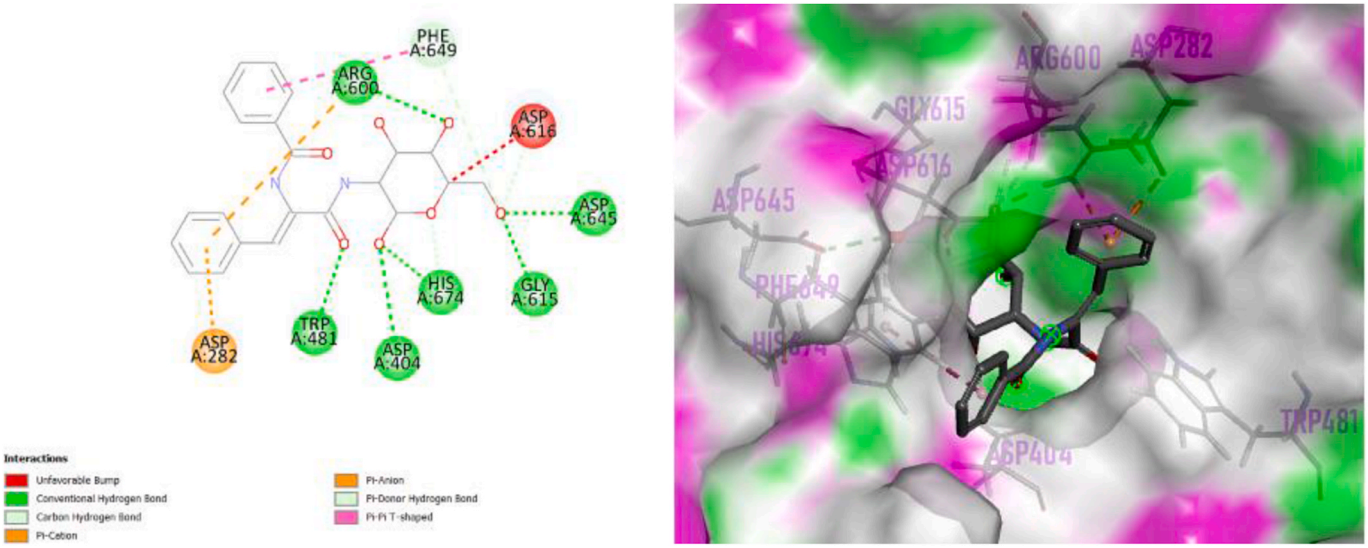

Fig. 10. 2D and 3D interactions of the newly designed scaffold with the α-glucosidase enzyme.

Table 2
Illustrates the predicted pharmacological properties of the new scaffold.

Physicochemical parameters										
Comp	**IC_{50}(nM)**	**Gold Score fitness**	**MW**	**Flexibility (#rotatable bonds)**	**Polarity (TPSA)**	**Lipophilicity (XLOGP3)**	**Insolubility (ESOL Log S)**	**Insaturation (Fraction Csp^3)**	**#Lipinski violations**	
New Scaffold	–	62.73	428.44	8	148.35	0.54	−2.59	0.27	1	
ADME parameters										
	Log K_p(Cm/s)	**GI absorption**	**BBB permeant**	**P-gp substrate**	**CYP1A2 inhibitor**	**CYP2C19 inhibitor**	**CYP2C9 inhibitor**	**CYP2D6 inhibitor**	**CYP3A4 inhibitor**	
	−8.53	Low	No	Yes	No	No	No	No	No	

clinically used drugs by adding or removing specific functional groups, such as hydroxylation, demethylation, and dealkylation [19]. As per Lipinski's rule, a drug is considered drug-like if it violates no more than one of the following criteria: 1) No more than 5 HBDs; 2) No more than 10 HBAs; 3) Molecular weight (MW) less than 500 Da; or 4) Calculated octanol-water partition coefficient (C log P) not exceeding 5 [20]. All the studied compounds adhere to Lipinski's rule, which has implications for oral bioavailability, metabolism, clearance, toxicity, and in vitro pharmacology. Furthermore, none of the compounds exhibited permeability through the blood-brain barrier. Table S5 provides the evaluated parameters. Among the 20 compounds, 8, including 1b, 3b, 4b, 5b, 6b, 7b, 1c, and 2d, showed better GoldScore fitness than acarbose and complied with Lipinski's rules. As shown in Fig. S17, compounds 1b, 2b, 3b, 4b, 5b, 6b, 7b, and 4d display a favorable physicochemical profile for oral bioavailability, assessed through a hexagonal diagram encompassing parameters such as lipophilicity, molecular weight, polarity (TPSA), solubility (log S), saturation (Csp^3 fraction), and flexibility (number of rotatable bonds).

3.5. Rational design of new scaffold and analysis

In this study, we used pharmacophore modeling with Pharmit to screen the BindingDB database for compounds with potential α-glucosidase inhibitory activity. Molecular docking simulations identified optimal binding interactions and key functional groups contributing to strong binding affinity. A subset of selected compounds then underwent 3D-QSAR modeling, pinpointing functional groups that enhance inhibitory activity. Based on these findings, we designed a novel scaffold using fragment replacement methods, incorporating a glycosyl group for optimal binding within the protein's pocket, an amin group to enhance binding affinity, and two phenyl groups to increase inhibitory activity, as supported by QSAR results (Fig. 8). The novel scaffold demonstrated a high GoldScore of 62.73 for α-glucosidase, surpassing all other ligands evaluated, indicating selective inhibition potential comparable to acarbose and other compounds. Fig. 9 illustrates the two- and three-dimensional interactions between the scaffold and α-glucosidase, highlighting frequent hydrogen bonds from the aminoglycosyl structure and additional favorable aromatic interactions. The interaction analysis reveals that the new scaffold retains key hydrogen bonds with ASP616, ARG600, and TRP481, similar to acarbose, while also exhibiting additional π-cation and π-π interactions with ASP282 and PHE649 that may enhance binding stability (see Fig. 10).

Pharmacological profiling revealed favorable drug-like properties for the scaffold, with predicted solubility (log S = −2.59) indicating adequate aqueous solubility, and low lipophilicity (log P = 0.54), likely due to hydroxyl groups, enhancing safety. The compound meets several drug-likeness criteria, including flexibility (8 rotatable bonds), saturation (sp^3 carbon fraction = 0.27), and TPSA (148 $Å^2$), which, though slightly above the ideal threshold, remains suitable for target-specific binding. Importantly, the scaffold is not predicted to cross the blood-brain barrier, reducing central nervous system-related risks, and shows low gastrointestinal absorption. Additionally, as a P-glycoprotein substrate, the scaffold may benefit from enhanced intestinal distribution without inhibiting cytochrome P450 isoforms, thus minimizing drug-drug interactions—an essential consideration for diabetes management.

The pharmacological properties of the scaffold, summarized in Table 2 confirm compliance with desirable criteria, including lipophilicity, polarity, molecular weight, solubility, and flexibility. Based on these results, the new scaffold is anticipated to have comparable or superior biological activity to acarbose, with reduced side effects, enhancing its therapeutic potential as a selective AGI.

3.6. Molecular dynamics simulation analysis

3.6.1. RMSD

To examine the stability of the systems during 100 ns of MD

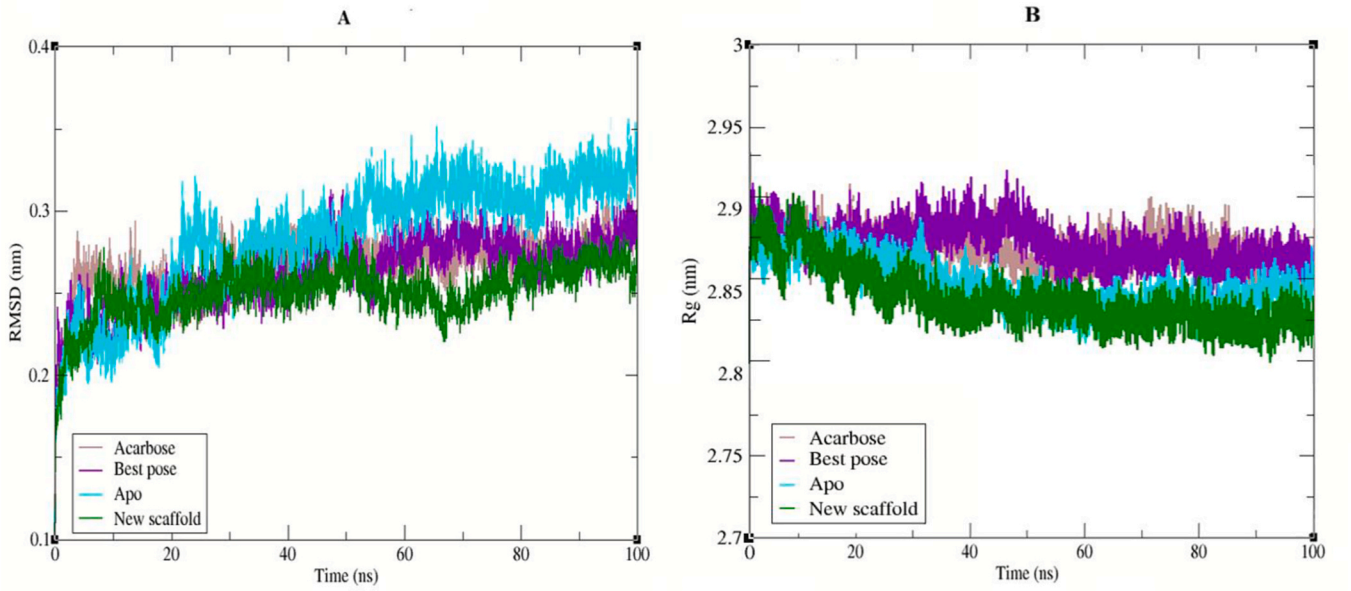

Fig. 11. A) RMSD and B) R_g plots of four simulations.

simulations, the RMSD changes of the backbone atoms for the protein in four different states include protein in water (Apo), protein-acarbose complex as the reference, protein complexed with the best pose of docking, and protein in complex with the newly designed scaffold; were calculated and are shown in Fig. 11. The new scaffold complex shows the lowest RMSD values throughout the simulation, staying consistently around 0.2–0.25 nm. This low RMSD suggests that the new scaffold binds to alpha-glucosidase in a highly stable manner, minimizing fluctuations in the protein backbone. The low and consistent RMSD values indicate that the protein structure remains relatively unchanged upon binding the new scaffold, reflecting a stable and favorable interaction. This stability suggests that the scaffold effectively inhibits structural fluctuations, potentially enhancing the inhibitory effectiveness.

The acarbose complex shows moderate RMSD values, generally between 0.25 and 0.3 nm, but with more fluctuations compared to the new scaffold complex. This trend suggests that, while acarbose stabilizes the protein to some extent, it does not achieve the same level of structural restraint as the new scaffold. The fluctuations observed in the acarbose complex could indicate weaker or less optimal interactions with alpha-glucosidase compared to the new scaffold, which may affect its overall binding affinity and inhibitory activity. The apo form exhibits the highest RMSD values, rising above 0.3 nm and displaying substantial fluctuations throughout the simulation. This result is expected, as the absence of a ligand allows the protein to adopt more flexible conformations, leading to greater structural deviations. The best docking pose complex (purple) shows intermediate stability between acarbose and the new scaffold, with RMSD values close to 0.3 nm. While it demonstrates more stability than the apo form, it does not perform as well as the new scaffold, suggesting that the scaffold design was successful in enhancing binding stability and inhibitory potency.

3.6.2. *Radius of gyration analysis (R_g)*

The radius of gyration (R_g) provides insights into the compactness and structural stability of alpha-glucosidase in the presence of different

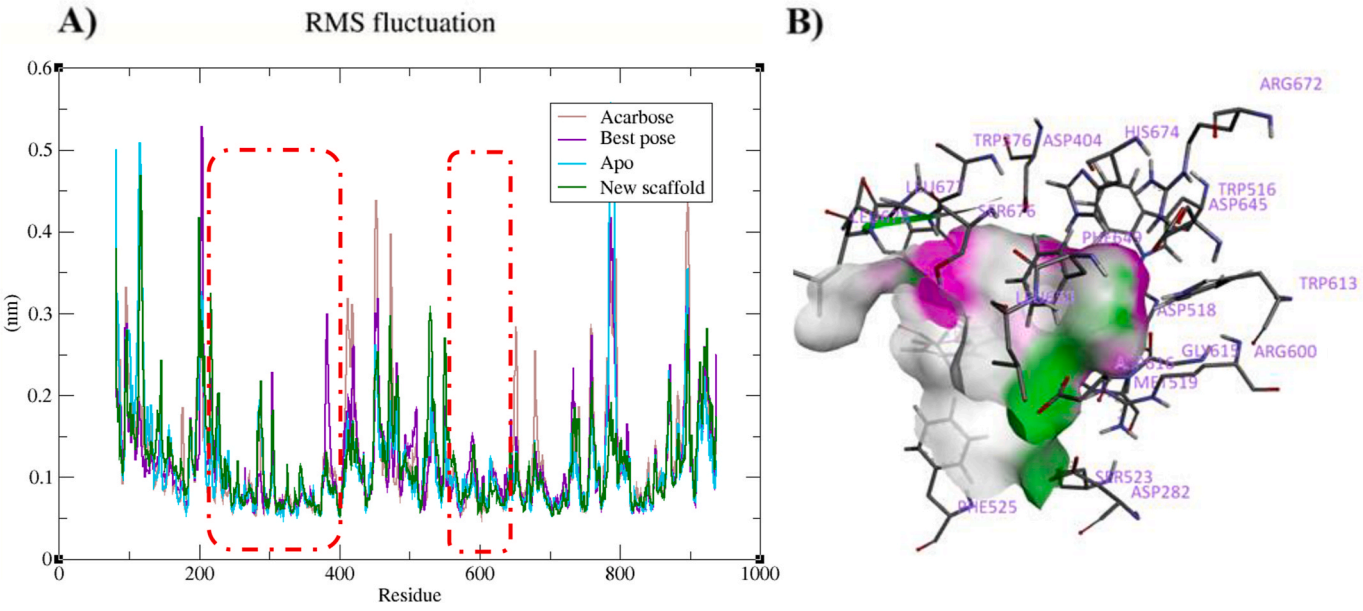

Fig. 12. A) RMSF plots and B) 3D view of cavity of enzyme.

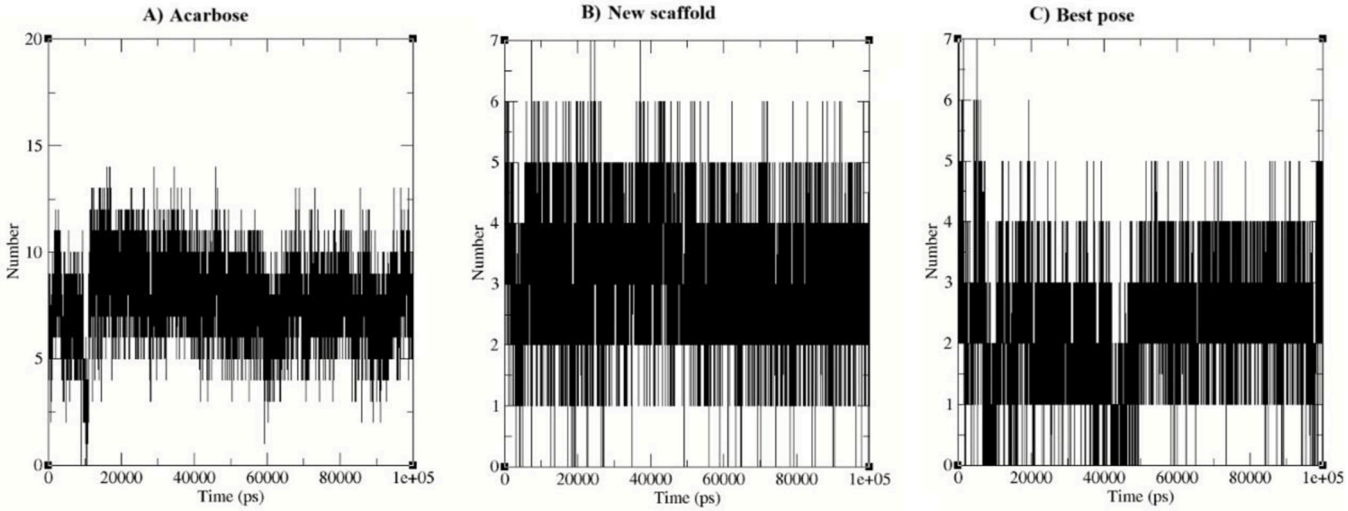

Fig. 13. Hydrogen bond analysis of A) acarbose in comparison with B) new scaffold and C) best pose.

ligands (Fig. 11). For the apo form, the R_g averaged approximately 2.85 nm with minimal fluctuations, indicating a stable and compact structure in the absence of ligands, serving as a baseline for comparison. The acarbose-bound complex showed a slightly higher R_g, around 2.87 nm, with increased fluctuations, suggesting subtle structural expansion due to conformational adjustments upon ligand binding.

In the best-docked pose complex, the R_g was similar to that of acarbose, averaging around 2.9 nm, indicating some structural relaxation likely due to ligand interactions, with a slightly less compact structure. The newly designed scaffold exhibited the lowest R_g among all complexes, averaging approximately 2.8 nm. This reduction suggests a more compact and stable protein conformation in the presence of the scaffold, likely due to stronger and more stabilizing interactions. The consistently lower R_g values imply that the scaffold may better preserve alpha-glucosidase's structural integrity compared to acarbose or the best docked pose.

3.6.3. RMSF

The RMSF plot illustrates the flexibility of residues within the alpha-glucosidase enzyme. Each curve indicates the mobility of specific residues, providing insight into the stability of the protein's structure in each complex.

The new scaffold (green curve) reduces fluctuations in several regions of alpha-glucosidase, particularly around residues crucial to the active site. This stabilization effect suggests that the scaffold forms strong interactions with these residues, maintaining the structural integrity of the binding pocket. Lower RMSF values indicate a more stable binding environment, which can enhance inhibitory activity by reducing protein conformational changes that might weaken binding affinity.

Fig. 12B shows key residues in the active site, including TRP516, ASP404, ASP518, ARG600, TRP613, ASP616, SER523, and PHE525, interacting with the scaffold. These residues are known for their roles in catalysis and substrate binding. In the presence of the new potent inhibitor, these residues exhibit lower RMSF values, indicating reduced flexibility. This reduction suggests that the scaffold is effectively anchoring these residues, enhancing stability within the active site and potentially increasing binding affinity. Residues like TRP516, TRP613, PHE525, and LEU650 likely engage in hydrophobic interactions with the scaffold, which helps stabilize the complex. The presence of hydrophobic interactions is consistent with lower RMSF values in these regions. Key residues like ASP404, ASP518, and SER523 are known to form hydrogen bonds, which are critical for ligand binding. The lower RMSF values for these residues suggest that the scaffold is forming stable hydrogen bonds, further contributing to the stability of the active site configuration. In comparison with Acarbose, although acarbose also reduces RMSF in certain regions, the new scaffold shows a more pronounced reduction across several critical residues, as seen in the RMSF plot. This suggests that the scaffold has a stronger stabilizing effect on the protein's active site, potentially making it a more potent inhibitor.

3.6.4. H-bonds

Fig. 13 compares hydrogen bond interactions over time between the enzyme and three ligands. Acarbose exhibits the highest average number of hydrogen bonds, fluctuating between 5 and 15, with a mean value of 7.73, indicating strong and dynamic interactions that contribute to its known efficacy as an inhibitor. In contrast, the new scaffold and the best docking pose form 3.19 and 2.27 hydrogen bonds on average, respectively. Despite having fewer hydrogen bonds than Acarbose, these ligands maintain consistent interactions, suggesting stable binding within the active site. This reduced hydrogen bonding in the scaffold, compared to Acarbose, may correlate with fewer side effects, aligning with its design purpose.

The analysis of the donor-acceptor distance distribution in hydrogen bonds (Fig. S18) indicates that acarbose and the new scaffold exhibit similar probability density in both intensity and range, whereas the best pose has a lower and broader distribution. This suggests that the likelihood of hydrogen bond formation in the best pose is lower compared to the other two ligands, and the formed bonds are less stable.

To evaluate hydrogen bond stability, we analyzed the occupancy of

Table 3
Hydrogen bond occupancy of key amino acids in the binding site for the new scaffold, best pose, and acarbose (values below 5 % are shown as zero).

Hydrogen Bond Occupancy%							
	Aspartic acid-282	Aspartic acid-404	Aspartic acid-518	Methionine-519	Arginine-600	Aspartic acid-616	Aspartic acid-645
New scaffold	0	0	0	36.2	42.54	69.83	73.62
Best pose	0	5.88	0	0	0	12.35	0
Acarbose	92.63	78.96	93.48	0	0	0	0

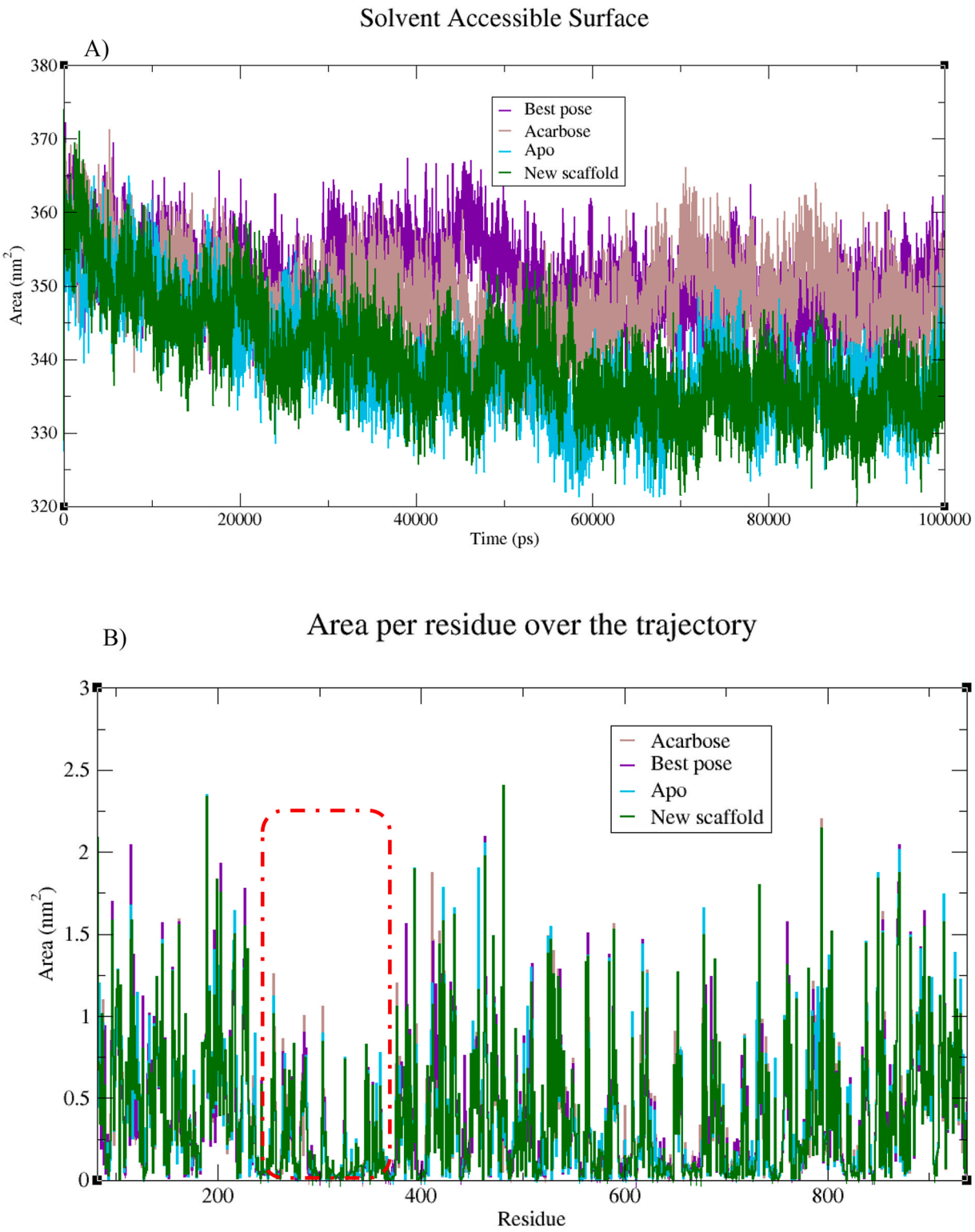

Fig. 14. A) Solvent Accessible Surface Area (SASA) analysis per time and B) SASA per residue for four complexes during 100 ns simulation.

23 key amino acids in the binding site throughout the simulation, calculating the presence or absence of hydrogen bonds as a percentage. A 3.5 Å distance cutoff and 30° angle threshold were applied, considering both donor and acceptor interactions. The results highlight that acarbose forms the most stable interactions, with Asp-282, Asp-404, and Asp-518 showing high occupancy (>70 %), confirming its strong binding stability. The best pose exhibits weak interactions, with only Asp-404 (5.88 %) and Asp-616 (12.35 %) forming hydrogen bonds, indicating lower stability. The new scaffold forms stable hydrogen bonds, particularly with Methionine-519 (36.2 %), Arginine-600 (42.54 %), Asp-616 (69.83 %), and Asp-645 (73.62 %), which contributes to a consistent average number of hydrogen bonds, supporting its potential binding stability. Table 3 summarizes the hydrogen bond occupancy for the most significant interactions. Overall, these findings support the scaffold's potential as a promising lead compound with an optimized balance of efficacy and safety.

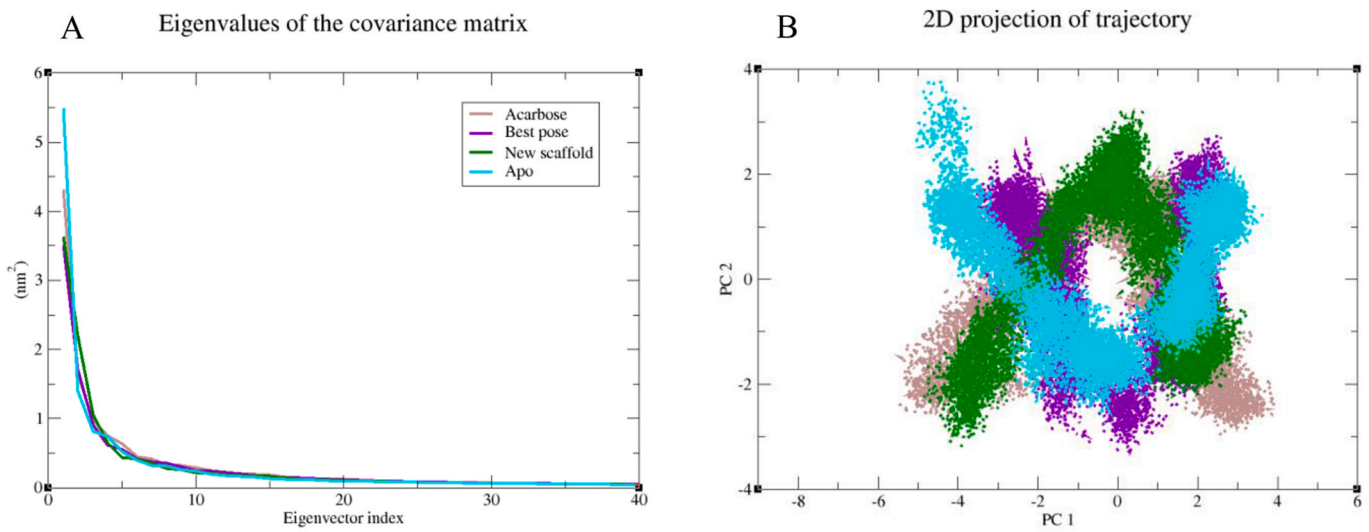

Fig. 15. PCA-Principal component analysis (A) Plots of eigenvalues in first 40 eigenvectors. (B) First two eigenvectors describing the protein motion in phase space for all the complexes.

3.6.5. Solvent accessible surface area (SASA)

SASA is a crucial parameter in protein structure analysis, providing insights into protein folding, stability, and intermolecular interactions. Fig. 14A shows the solvent-accessible surface area (SASA) over 100 ns, which measures the portion of the protein surface accessible to solvent molecules. Across all complexes, we observed surface areas from 330 to 370 nm^2, with the new scaffold exhibiting slightly lower values, suggesting a more compact conformation and reduced solvent exposure. As shown in the red-marked region in Fig. 14B, the accessible surfaces have significantly decreased, corresponding to the binding site residues. This observation indicates that all ligands are well-positioned within the binding site, preventing water molecules from penetrating these regions.

3.6.6. Essential dynamics analysis

To gain deeper insight into the global motions and dynamic behavior of the protein–ligand complexes, we performed principal component analysis (PCA) on the molecular dynamics (MD) trajectories. The covariance matrix of Cα atomic fluctuations was diagonalized, and the eigenvalues for the first 40 eigenvectors are shown in Fig. 15A. The highest eigenvalues correspond to the most significant collective motions. Notably, almost all eigenvalues are at a similar level, indicating that no distinct conformational transitions are observed.

To visualize how each system explores conformational space, we projected the trajectories onto the first two principal components (PC1 and PC2), as illustrated in Fig. 15B. The contribution percentages of the data along PC1 to PC3 for the four simulations are approximately 30 %, 10 %, and 6 %, respectively. This indicates that PC1, which reflects the alpha-carbon fluctuations, is not sufficiently large to capture the conformational changes of the protein from one conformation to another. As expected, PC2, which is smaller than PC1, likely reflects the fluctuations across the protein backbone. However, we cannot infer significant structural changes along the second principal component as we observed for the first component. Nonetheless, it can be stated that the apo form and the protein-ligand complexes show a slight change in rigidity, with the protein-ligand complexes maintaining limited flexibility in comparison to the apo form. Overall, these results align with our RMSD and RMSF findings, reinforcing that our scaffold complex retains essential stability while limiting excessive conformational changes. This stable dynamic profile may contribute to its binding affinity and provides further support for its potential as a promising α-glucosidase inhibitor.

3.6.7. Binding free energy analysis molecular mechanics Poisson–Boltzmann surface area calculation

The binding free energy components of the protein-ligand complexes were analyzed to evaluate the stability and binding affinity of the newly designed scaffold compared to the best docking pose and the reference inhibitor. These calculations were performed using the MM-PBSA method with g_mmpbsa tools, which estimate the free energy of endpoint states without requiring intermediate state simulations. This approach integrates molecular mechanical energies with continuum solvent models. The total ΔG_bind was determined by assessing the free

Table 4
Binding energy components for protein-ligand complexes against α-glucosidase and α-amylase.

Binding Free Energy Components						
Protein-Ligand Complexes	Van Der Waals Energy (kJ/mol)	Electro static Energy (kJ/mol)	Polar solvation Energy (kJ/mol)	SASA Energy (kJ/mol)	Binding free Energy (kJ/mol)	Binding free Energy (kcal/mol)
α-glucosidase-New scaffold	−168.297 ± 14.548	−53.640 ± 14.004	148.725 ± 21.760	−18.460 ± 1.233	−91.673 ± 20.547	−21.909 ± 4.910
α-glucosidase-Best pose	−142.200 ± 13.829	−47.085 ± 17.168	124.533 ± 20.368	−16.903 ± 1.235	−81.654 ± 14.788	−19.515 ± 3.531
α-glucosidase-Acarbose	−182.583 ± 17.048	−112.072 ± 22.178	207.918 ± 34.563	−20.284 ± 1.456	−107.022 ± 24.171	−25.578 ± 5.783
α-amylase-New scaffold	−162.522 ± 31.265	−31.265 ± 15.783	157.552 ± 47.894	−20.255 ± 3.700	−56.490 ± 18.962	−13.501 ± 4.532
α-amylase-Best pose	−143.480 ± 21.190	−31.472 ± 18.565	115.368 ± 45.807	−17.898 ± 2.303	−77.482 ± 18.216	−18.518 ± 4.354
α-amylase-Acarbose	−127.974 ± 18.141	−31.017 ± 16.558	108.702 ± 30.328	−15.839 ± 2.092	−66.127 ± 17.792	−15.804 ± 4.252

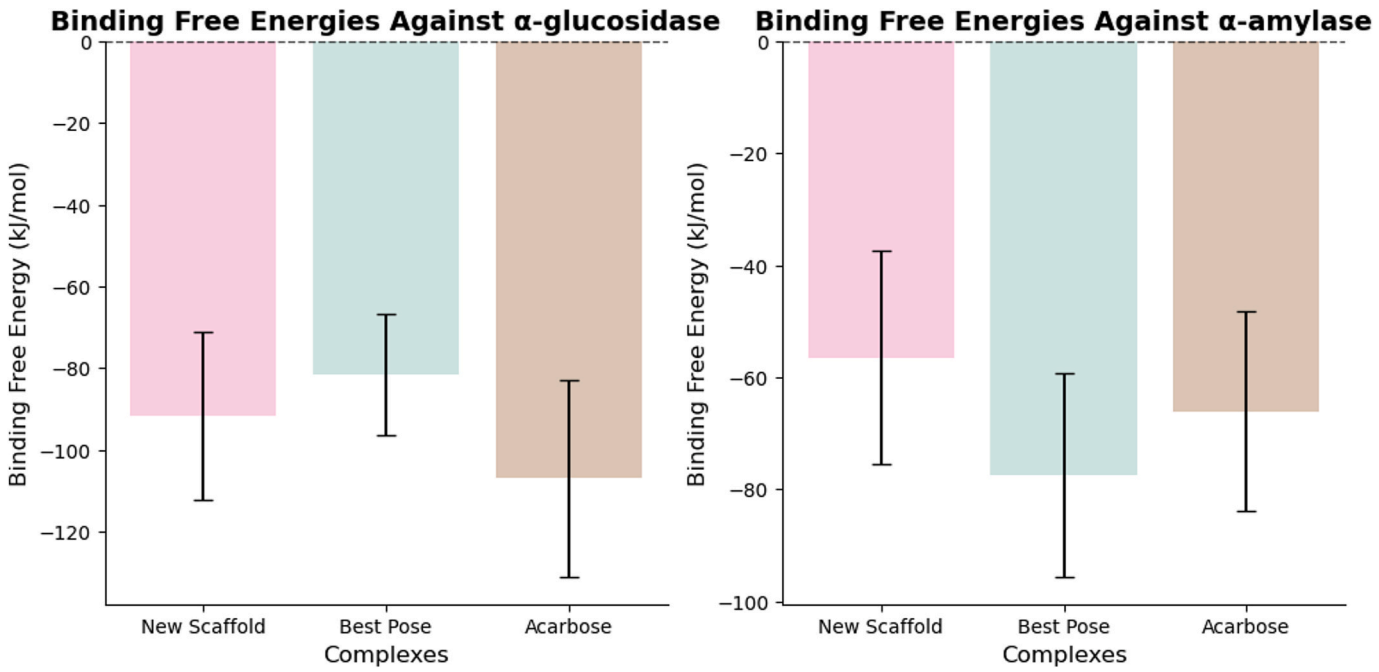

Fig. 16. Binding free energy comparison of three complexes against **α-glucosidase and α-amylase.**

potential energy and solvation energy of each protein-ligand complex.

To investigate molecular interactions at the active site, binding free energy (ΔG) was computed, incorporating bonded and non-bonded interactions, including van der Waals and electrostatic forces. MM-PBSA calculations were conducted on 1000 evenly spaced frames extracted from 10,000 frames obtained in molecular dynamics (MD) simulations. The results, summarized in Table 4 and visualized in Fig. 16, provide insights into the energetic contributions governing ligand binding.

The MM-PBSA analysis indicates that the new scaffold exhibits a stable interaction with α-glucosidase, with a binding free energy of −91.67 kJ/mol. In contrast, Acarbose demonstrates a stronger binding affinity (−107.02 kJ/mol), suggesting a more stable complex. However, given the margin of error, the binding affinities of all complexes remain within a comparable range. Notably, inhibitory activity assays (Table S5) reveal that the best docking pose exhibits significantly greater inhibitory potency than Acarbose, suggesting that the modified scaffold may offer enhanced activity.

Since α-amylase hydrolyzes polysaccharides into oligosaccharides and disaccharides, while α-glucosidase further converts them into glucose, inhibiting both enzymes can delay glucose absorption into the bloodstream [25]. However, α-amylase inhibition is associated with increased secretion of undigested carbohydrates into the large intestine, leading to gastrointestinal side effects—a common drawback of α-glucosidase inhibitors like Acarbose [26].

To evaluate enzyme selectivity, molecular dynamics simulations were performed for complexes with α-amylase. The new scaffold exhibited lower binding affinity for α-amylase (−56.49 kJ/mol) compared to the best docking pose (−77.48 kJ/mol) and Acarbose (−66.13 kJ/mol). This suggests that the new scaffold may act as a more selective α-glucosidase inhibitor, potentially reducing gastrointestinal side effects associated with α-amylase inhibition.

4. Conclusions

This study employed computational techniques include Pharmacophore modeling, molecular docking, and 3D-QSAR analysis, to identify and design new potent AGIs for diabetes management. Pharmacophore modeling confirmed that glycosyl group are essential for binding interactions with α-glucosidase active-site residues. Key features identified included two HBAs, three HBDs, and an ionizable center contributed by hydroxyl and amine groups. The 3D-QSAR demonstrated reliable statistical quality according to the q2 and r2 values for CoMFA and CoMFA-RF. The final results of contour map interpretation indicated that the presence of electron-donating groups, such as phenyl and benzamide, increases biological activity. Docking studies showed that compounds 1–14 had strong inhibitory effects, with GoldScore fitness values between 50.58 and 60.57, surpassing the acarbose reference. These compounds contained glucosyl and aromatic groups, which played a crucial role in their binding affinity and inhibitory potential. Using a fragment-based approach, the new scaffold was designed by retaining the glucosyl structure, given its critical role in widely used marketed drugs (as shown in the graphical abstract), and incorporating key hydrogen bond donor and acceptor features from hydroxyl functional groups. Additionally, a benzamide group and a benzene ring were introduced based on QSAR results, which predict an enhancement in inhibitory activity. MD simulations confirmed the stability of the new scaffold against alpha-glucosidase, demonstrating a lower RMSD than other compounds, reduced binding site fluctuations, stable hydrogen bonding throughout the simulation, and a well-maintained solvent-accessible surface area (SASA), collectively indicating strong and sustained binding. Furthermore, MM-PBSA analysis of the three complexes against α-glucosidase and α-amylase suggests that the new scaffold is likely to exhibit inhibitory activity comparable to the best docking pose, which demonstrated the highest inhibitory potency in the binding database. Additionally, the new scaffold shows higher binding affinity for α-glucosidase while exhibiting weaker binding to α-amylase compared to the other compounds. This selectivity suggests a lower likelihood of gastrointestinal side effects, a common concern associated with α-amylase inhibition. Additionally, pharmacokinetic assessments revealed favorable drug-likeness and ADME properties, alongside a strong binding affinity (GoldScore = 62.73), reinforcing the scaffold's therapeutic potential for diabetes treatment. These findings underscore the effectiveness of rational drug design in optimizing AGI efficacy and position the newly developed scaffold as a strong candidate for further validation through in vitro enzyme inhibition assays, in vivo studies, and machine learning-based predictive models to further refine and optimize its design.

Data availability

The data supporting the findings of this study is not available.

Statement of usage of artificial intelligence

This study utilized artificial intelligence tools, including ChatGPT, solely for grammar checking and enhancing the fluency of the manuscript. No AI tools were involved in generating content, analyzing results, or developing software. After using this tool, the authors reviewed and edited the content as needed and take full responsibility for the content of the publication.

Funding information

The authors acknowledge the University of Tehran for providing research facilities. This research was financially supported by Iran National Science Foundation (INSF) under grant number 96005880.

Declaration of competing interest

The authors declare that they have no known competing financial interests or personal relationships that could have appeared to influence the work reported in this paper.

Appendix A. Supplementary data

Supplementary data to this article can be found online at https://doi.org/10.1016/j.bbrep.2025.101995.

Data availability

Data will be made available on request.

References

[1] S.K. Liu, H. Hao, Y. Bian, Y.X. Ge, S. Lu, H.X. Xie, K.M. Wang, H. Tao, C. Yuan, J. Zhang, J. Zhang, Discovery of new α-glucosidase inhibitors: structure-based virtual screening and biological evaluation, Front. Chem. 9 (2021) 639279, https://doi.org/10.3389/fchem.2021.639279.

[2] K.H. Yoon, J.H. Lee, J.W. Kim, J.H. Cho, H.Y. Choi, S.H. Ko, P. Zimmet, H.Y. Son, Epidemic obesity and type 2 diabetes in Asia, Lancet 368 (2006) 1681–1688, https://doi.org/10.1016/S0140-6736(06)69703-1.

[3] K.M. Gillespie, Type 1 diabetes: pathogenesis and prevention, Can. Med. Assoc. J. 157 (2006) 165–170, https://doi.org/10.1503/cmaj.060244.

[4] L. Ye, O. Mueller, J. Bagwell, M. Bagnat, R.A. Liddle, J.F. Rawls, High fat diet induces microbiota-dependent silencing of enteroendocrine cells, Elife 8 (2019) e48479, https://doi.org/10.7554/eLife.48479.

[5] F. Azimi, H. Azizian, M. Najafi, G. Khodarahmi, L. Saghaei, M. Hassanzadeh, J. B. Ghasemi, M.A. Faramarzi, B. Larijani, F. Hassanzadeh, M. Mahdavi, Design, synthesis, biological evaluation, and molecular modeling studies of pyrazole-benzofuran hybrids as new α-glucosidase inhibitor, Sci. Rep. 11 (2021) 1–16, https://doi.org/10.1038/s41598-021-99899-1.

[6] S. Chiba, Molecular mechanism in α-glucosidase and glucoamylase, Biosci. Biotechnol. Biochem. 61 (1997) 1233–1239, https://doi.org/10.1271/bbb.61.1233.

[7] Z.P. Zhang, X.U.E. Wan-Ying, H.U. Jian-Xing, D.C. Xiong, W.U. Yan-Fen, Y.E. Xin-Shan, Novel carbohydrate-triazole derivatives as potential α-glucosidase inhibitors, Chin. J. Nat. Med. 18 (2020) 729–737, https://doi.org/10.1016/S1875-5364(20)60013-9.

[8] A.V. Veselovsky, A.S. Ivanov, Strategy of computer-aided drug design, Curr. Drug Targets: Infect. Disord. 3 (2003) 33–40, https://doi.org/10.2174/1568005033342145.

[9] F. Azimi, H. Azizian, M. Najafi, G. Khodarahmi, L. Saghaei, M. Hassanzadeh, J. B. Ghasemi, M.A. Faramarzi, B. Larijani, F. Hassanzadeh, M. Mahdavi, Design, synthesis, biological evaluation, and molecular modeling studies of pyrazole-benzofuran hybrids as new α-glucosidase inhibitor, Sci. Rep. 11 (2021) 20776, https://doi.org/10.1038/s41598-021-99899-1.

[10] J.B. Ghasemi, A. Abdolmaleki, F. Shiri, Molecular docking challenges and limitations, in: Pharmaceutical Sciences: Breakthroughs in Research and Practice, IGI Global, 2017, pp. 770–794, https://doi.org/10.4018/978-1-5225-1762-7.ch030.

[11] B. Usman, N. Sharma, S. Satija, M. Mehta, M. Vyas, G.L. Khatik, N. Khurana, P. M. Hansbro, K. Williams, K. Dua, Recent developments in alpha-glucosidase inhibitors for management of type-2 diabetes: an update, Curr. Pharm. Des. 25 (23) (2019) 2510–2525, https://doi.org/10.2174/1381612825666190717104547.

[12] Y. Zhang, H. Gao, R. Liu, L. Chen, X. Li, L. Zhao, et al., Quinazoline-1-deoxynojirimycin hybrids as high active dual inhibitors of EGFR and α-glucosidase, Bioorg. Med. Chem. Lett. 27 (18) (2017) 4309–4313, https://doi.org/10.1016/j.bmcl.2017.08.035PMID:28838691.

[13] G. Wang, Z. Peng, J. Wang, X. Li, J. Li, Synthesis, in vitro evaluation and molecular docking studies of novel triazine-triazole derivatives as potential α-glucosidase inhibitors, Eur. J. Med. Chem. 125 (2017) 423–429, https://doi.org/10.1016/j.ejmech.2016.09.067PMID:27689725.

[14] G. Wang, J. Wang, D. He, X. Li, J. Li, Z. Peng, Synthesis and biological evaluation of novel 1,2,4-triazine derivatives bearing carbazole moiety as potent α-glucosidase inhibitors, Bioorg. Med. Chem. Lett. 26 (12) (2016) 2806–2809, https://doi.org/10.1016/j.bmcl.2016.04.071PMID:27177827.

[15] M.L. Verdonk, J.C. Cole, M.J. Hartshorn, C.W. Murray, R.D. Taylor, Improved protein ligand docking using GOLD, Proteins 52 (2003) 609–623, https://doi.org/10.1002/prot.10465.

[16] Z. Bakherad, M. Safavi, A. Fassihi, H. Sadeghi-Aliabadi, M. Bakherad, H. Rastegar, M. Saeedi, J.B. Ghasemi, L. Saghaie, M. Mahdavi, Design and synthesis of novel cytotoxic indole-thiosemicarbazone derivatives: biological evaluation and docking study, Chem. Biodivers. 16 (2019) e1800470. Doi: 10.102/cbdv.201800470.

[17] O.F. Guner, J.P. Bowen, Setting the record straight: the origin of the pharmacophore concept, J. Chem. Inf. Model. 54 (2014) 1269–1283, https://doi.org/10.1021/ci5000533.

[18] J.S. Singh, S. Koushal, A. Kumar, S.R. Vimal, V.K. Gupta, Book Review: Microbial Inoculants in Sustainable Agricultural Productivity-Vol. II: Functional Application, 2016.

[19] C.B.R.d. Santos, C.C. Lobato, M.A.C. de Sousa, W.J.d.C. Macedo, J.C.T. Carvalho, Molecular modeling: origin, fundamental concepts and applications using structure-activity relationship and quantitative structure-activity relationship, Rev. Theor. Sci. 2 (2014) 91–115, https://doi.org/10.1166/rits.2014.1016.

[20] Y. Entezari Heravi, H. Sereshti, A.A. Saboury, J. Ghasemi, M. Amirmostofian, C. T. Supuran, 3D QSAR studies, pharmacophore modeling, and virtual screening of diarylpyrazole– benzene sulfonamide derivatives as a template to obtain new inhibitors, using human carbonic anhydrase II as a model protein, J. Enzym. Inhib. Med. Chem. 32 (2017) 688–700, https://doi.org/10.1080/14756366.2016.1241781.

[21] S. Dove, A. Buschauer, Improved alignment by weighted field fit in CoMFA of histamine H2 receptor agonistic imidazolyl propyl guanidines, Quant. Struct.-Act. Relat. 18 (1999) 329–341, https://doi.org/10.1002/(SICI)1521-3838(199910)18:4<329::AID-QSAR329>3.0.CO;2-V.

[22] K.A. Akinyede, H.A. Oyewusi, G.D. Hughes, O.E. Ekpo, O.O. Oguntibeju, In vitro evaluation of the anti-diabetic potential of aqueous acetone helichrysum petiolare extract (AAHPE) with molecular docking relevance in diabetes mellitus, Molecules 27 (1) (2021) 155, https://doi.org/10.3390/molecules27010155.

[23] A.K. Malde, L. Zuo, M. Breeze, M. Stroet, D. Poger, P.C. Nair, C. Oostenbrink, A. E. Mark, An automated force field topology builder (ATB) and repository: version 1.0, J. Chem. Theor. Comput. 7 (12) (2011) 4026–4037, https://doi.org/10.1021/ct200196m.

[24] Molecular Operating Environment (MOE), 2024.0601 Chemical Computing Group ULC, 910-1010 Sherbrooke St. W., Montreal, QC H3A 2R7, 2024.

[25] S. Chiba, Molecular mechanism in α-glucosidase and glucoamylase, Biosci. Biotechnol. Biochem. 61 (8) (1997) 1233–1239, https://doi.org/10.1271/bbb.61.1233.

[26] A.H.M. Lin, B.R. Hamaker, B.L. Nichols Jr, Direct starch digestion by sucrase-isomaltase and maltase-glucoamylase, J. Pediatr. Gastroenterol. Nutr. 55 (2012) S43–S45, https://doi.org/10.1097/01.mpg.0000421414.95751.be.